Drug delivery with microsecond laser pulses into gelatin

HanQun Shangguan, Lee W. Casperson, Alan Shearin, Kenton W. Gregory, and Scott A. Prahl

Photoacoustic drug delivery is a technique for localized drug delivery by laser-induced hydrodynamic pressure following cavitation bubble expansion and collapse. Photoacoustic drug delivery was investigated on gelatin-based thrombus models with planar and cylindrical geometries by use of one microsecond laser pulses. Solutions of a hydrophobic dye in mineral oil permitted monitoring of delivered colored oil into clear gelatin-based thrombus models. Cavitation bubble development and photoacoustic drug delivery were visualized with flash photography. This study demonstrated that cavitation is the governing mechanism for photoacoustic drug delivery, and the deepest penetration of colored oil in gels followed the bubble collapse. Spatial distribution measurements revealed that colored oil could be driven a few millimeters into the gels in both axial and radial directions, and the penetration was less than 500 μm when the gelatin structure was not fractured.

Key words: Ablation, photoacoustic transients, localized drug delivery, cavitation bubble, laser thrombolysis.

1. Introduction

Pharmacological therapy for the treatment of restenosis, thrombosis, and ischemic heart diseases may eventually become clinically practical through the localized delivery of therapeutic agents.[1–3] A primary advantage of localized drug delivery over traditional drug delivery is that, with the former, side effects such as bleeding and stroke can be avoided, because high concentrations of pharmacologic agents are delivered directly to the treatment site with minimal systemic exposure to the medication. Localized drug delivery for vascular applications is typically achieved by use of balloon-based catheter systems.[2,4–7] For example, a double-balloon catheter is used for delivering drug into vessel wall tissue by inflation of two balloons in an artery with a pressurized drug-filled volume between them.[2] The primary problems associated with current investigational systems are their cumbersome size and long inflation times as well as the risk of medial injury occurring during the balloon inflation process, thus potentially limiting the benefits of localized drug delivery.

Photoacoustic drug delivery is a technique for delivering drugs to localized areas.[8,9] Unlike the techniques for enhancing local delivery of molecules that use laser-induced shock waves,[10,11] photoacoustic drug delivery uses a laser pulse to generate a cavitation bubble in a blood vessel owing to the absorption of laser energy by targets (e.g., blood clots) or surrounding liquids (e.g., blood). The cavitation bubble expands and collapses hundreds of microseconds after the laser pulse. The hydrodynamic pressure arising from the expansion and collapse of the cavitation bubble can force the drug into the clot or the vessel wall. One can perform photoacoustic drug delivery by timing the laser pulses to be coincident with an injected bolus of drug. The delivery system for photoacoustic drug delivery could consist of only two elements: an optical fiber or light guide for delivering laser pulses and catheter tubing for injecting drugs. A fluid-core laser catheter has been used to remove thrombus (blood clot) with a pulsed dye laser without damaging the vessel

H-Q. Shangguan is with the Department of Electrical Engineering, Portland State University, Portland, Oregon 97201, and the Oregon Medical Laser Center, Portland, Oregon 97225. L. W. Casperson is with the Department of Electrical Engineering, Portland State University, Portland, Oregon 97201. A. Shearin is with the Oregon Medical Laser Center, Portland, Oregon 97225, and Palomar Medical Technologies, Inc., Beverly, Massachusetts 01915. K. W. Gregory and S. A. Prahl are with the Oregon Medical Laser Center, Portland, Oregon 97225, and Oregon Health Sciences University, Portland, Oregon 97201.

Received 20 November 1995.
0003-6935/96/193347-11$10.00/0

a fluid-core laser catheter may be an alternative method to current techniques for localized drug delivery.

Previous studies have established that cavitation bubbles can be formed in a liquid or on a solid target, depending on where the laser energy is absorbed. Cavitation bubbles play an important role in pulsed laser ablation of tissue and in laser lithotripsy.[13–16] Van Leeuwen *et al.* demonstrated that cavitation bubbles make it possible to ablate tissue in a noncontact mode through a layer of blood or saline, and the forceful expansion of a cavitation bubble induces mechanical damage in adjacent tissue in the form of dissections.[13] A study by Vogel *et al.* suggested that cavitation-induced dilatation of vessel walls occurring in pulsed laser angioplasty can be prevented by division of the laser pulse energy into a prepulse with low energy and an ablation pulse with high energy.[14] Rink *et al.* reported that cavitation bubble collapse is the governing factor for fragmentation and disruption during laser lithotripsy with microsecond laser pulses.[15] The stone is progressively fragmented by stresses exceeding its tensile strength and by fatigue. In clinical trials of laser thrombolysis, Gregory suggested that the removal of thrombus might be attributed to the acoustic phenomena from vaporization and ejection of materials.[17] Francis *et al.* recently demonstrated that ultrasound could be used to accelerate the transport of fibrinolytic agents into clots as a result of the ultrasound effects mediated by cavitation and microstreaming.[18] However, whether the laser-induced hydrodynamic pressure can be used to drive drugs into thrombus or tissue for localized drug delivery remained to be investigated.

This study was motivated by the possibility of using laser-induced hydrodynamic pressure to drive clot-dissolving enzymes into clots or vessel wall tissue for the enhancement of laser thrombolysis. Specifically, the aim of this study has been to identify the mechanisms of photoacoustic drug delivery through investigating how the target material, laser energy, absorption coefficient, fiber size, repetition rate, and number of pulses affect the spatial distribution of photoacoustically delivered drug. The process of photoacoustic drug delivery was visualized by use of flash photography, and the acoustic pressure transients were measured with a piezoelectric polyvinylidene fluorid (PVDF) transducer.

Photoacoustic drug delivery was studied with gelatin-based thrombus models that eliminated the biological variation of thrombus and provided transparent samples for spatial distribution measurement. Solutions of a hydrophobic red dye in mineral oil were irradiated with a microsecond laser pulse to initiate drug delivery. We found that photoacoustic drug delivery was associated with cavitation bubble formation and sound emission and that the deepest penetration followed the collapse of the cavitation bubble.

A. Laser Delivery

A flash-lamp-pumped dye laser (Palomar Medical Technologies) operating at 504 nm was used to create cavitation bubbles (Fig. 1). This wavelength corresponded to the peak absorption of the light-absorbing dye used. The pulse duration was 1.3 μs (full width at half-maximum). The laser energies varied from 30 to 100 mJ. Pulse-to-pulse energy variation was less than 5%. The repetition rate ranged from 1 to 10 Hz. The laser pulses were delivered by means of step-index fused-silica optical fibers with 300–1000-μm core diameters. The light was always absorbed by the liquid surrounding the fiber tip. Three irradiation configurations were used. First, a flat optical fiber tip was perpendicular to a planar target [Fig. 2(a)]. Second, a flat optical fiber tip was coaxial with a cylindrical channel [Fig. 2(b)]. Third, a side-firing fiber (MicroQuartz Sciences) was coaxial in a cylindrical channel but with irradiation perpendicular to the axis of the channel [Fig. 2(c)].

B. Preparation of Thrombus Models

The thrombus was modeled with 3.5% gelatin (60–300 bloom). The percentage was determined by the weight ratio of gelatin to water. The bloom number is the standard method for indicating the toughness of gels and is a measure of surface tension. Higher bloom numbers indicate stronger gels. No attempt was made to correlate the bloom number with any specific clots in this study, although the range studied was similar to that of typical clot toughness. The gelatin–water mixture was heated to 60 °C with stirring until it became clear. Liquid gelatin samples were poured into 1-cm cuvettes and molded to form 2–3-cm-thick thrombus models with planar or cylindrical geometries. To simulate cardiovascular applications, the channels were constructed ~2 mm in diameter under the assumption that some narrowing of the normal 2–4-mm adult human coronary artery is likely in a thrombotic lesion. The

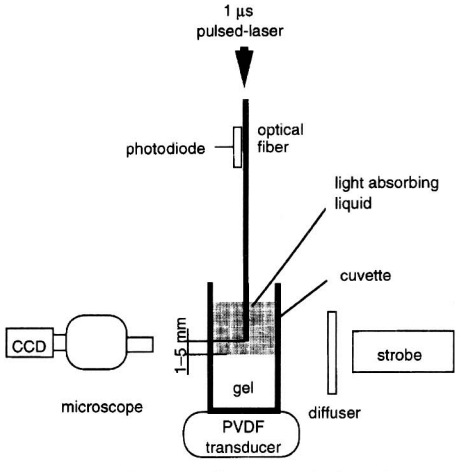

Fig. 1. Experimental setup for spatial distribution measurement, flash photography, and acoustic pressure measurement.

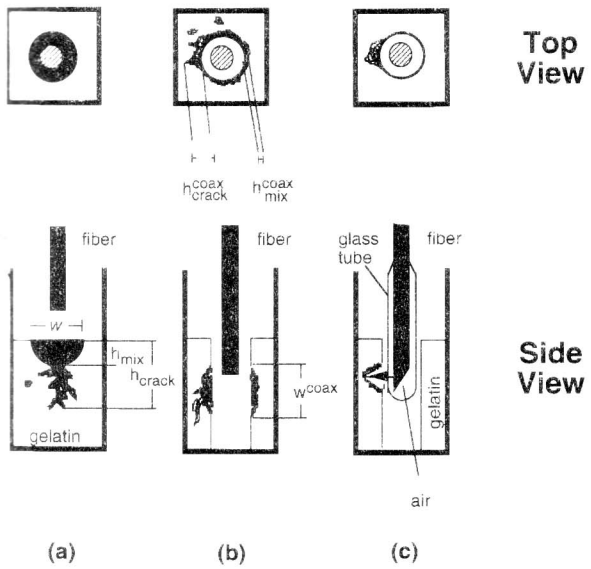

Schematic illustration of three irradiation configurations the methods used for measuring the spatial distribution of acoustically delivered dye in clear gels. The top and side of samples irradiated by perpendicular, coaxial, and side iation are shown in (a), (b), and (c), respectively.

amples were transparent, and it was easy to use ht microscopy to discriminate any colored sub- nces from clear gelatin.

Preparation of Drug Models

e used solutions of a hydrophobic dye (D&C Red 17, Warner–Jenkinson) in mineral oil (Paddock aboratories) as a model for the drug. The hydro- obic dye was used because the gels were water sed and staining of the surface by the dye was ndesirable. We added the dye to the mineral oil to hieve the desired absorption coefficient. We ob- rved that no dye passively diffused into gelatin in ntrol samples. The absorption coefficient of a lution was linearly proportional to the concentra- on of the dye in the oil: 0.0367 g of dye in 30-mL l gave an absorption coefficient of 300 cm^{-1} at 504 m. The absorption coefficients in our experiments aried from 50 to 300 cm^{-1}. The dye–oil mixture as heated to 100 °C with stirring until the appear- nce became uniform and was then cooled to room emperature. A solution of 300 cm^{-1} was saturated t room temperature after 4 h when the dye began to precipitate, and the absorption coefficient dropped to 250 cm^{-1}. The use of a sonicator (Medelco) for 10 min after the dye–oil solution was heated delayed the precipitation time for at least another hour.

D. Spatial Distribution Measurement

1. *Planar Geometry*

All planar targets were covered with 1.5 cm of colored oil. The target was clear gelatin ~2 cm thick. Ten laser pulses were delivered through an optical fiber into the colored oil for each experiment except in the study involving pulse number, in which 10–100 pulses were delivered). The fiber tip was positioned 1–5 mm above the target surface, as shown in Fig. 1. The laser energy output was measured with a joulemeter (J50LP, Molectron Detector) before and after each irradiation. Following photoacoustic drug delivery, the samples were measured under a stereo-optical microscope (SZ6045, Olympus). The stained areas in the clear gels indicated the presence of photoacoustically delivered colored oil. Figure 2(a) shows how the spatial distributions of colored oil in the gelatin were measured. The stained areas consisted of two parts: a hemisphere with width w and height h_{mix} and some colored cracks extending a depth h_{crack}. The distances w, h_{mix}, and h_{crack} were measured on all four sides of each sample. The spatial distribution of the colored oil in the gels was measured as functions of laser energy (30–100 mJ), absorption coefficient of the oil (50–300 cm^{-1}), fiber size (300–1000 μm), gelatin strength (60–300 bloom), repetition rate (1–10 Hz), pulse number (1–100), and fiber position (1–5 mm above the ablated target).

2. *Cylindrical Geometry*

A clear gelatin sample with a 2-mm cylindrical channel was filled with colored oil. Fifty laser pulses were delivered coaxially through a cleaved fiber tip or perpendicularly through a side-firing fiber tip. The fiber tip was located in the middle of the channel. Following laser irradiation, the gel samples were carefully removed from the cuvette and then fixed in 10% formalin. They were then sectioned into 2-mm-thick slices through both the irradiated and the nonirradiated sites after the colored oil in the channel was washed away with the formalin. To assess whether the process of photoacoustic drug delivery could enhance intravascular recanalization, we measured the lumenal areas and then compared them with control data measured from nonirradiated sections. The uniform penetration of colored oil in the gels was defined as h^{coax}_{mix}, whereas the colored cracks underneath h^{coax}_{mix} were defined as h^{coax}_{crack}. The measuring method is shown in Fig. 2(b).

E. Visualization of Photoacoustic Drug Delivery

Photoacoustic drug delivery was visualized with flash photography (Fig. 1). A triggerable CCD camera (CV-251, Protec) was used to photograph the processes. Each picture was a single event and was repeated three times for each parameter set. The bubble size was reproducible to 5% before the bubble collapse. The appearance of cavitation bubbles varied widely after the bubble collapse. A strobe (MVS-2601, EG&G) with a 5-μs pulse duration (full width at half-maximum) was used for illumination at an adjustable delay time (10–5000 μs) controlled by a digital delay generator (DG535, Stanford Research Systems). The generator was triggered by the laser pulse by use of a photodiode (UDT Instruments) that was attached to the laser delivery fiber. The delay

the laser pulse and the peak of the flash of light from the strobe.

F. Acoustic Pressure Measurement

The acoustic pressure measurements were intended for relative measurements of the acoustic pressure transients created by different laser parameters. A PVDF transducer (Hydrosonics) with a rise time of ~1 μs was placed under the cuvette (Fig. 1). The acoustic signals were recorded on a digital storage oscilloscope (DSA 602A, Tektronix) through an amplifier (Hydrosonics). Only the maximum signals were recorded for the comparative study of the acoustic pressure transients.

G. Statistical Evaluation

All values are expressed as mean ± standard deviation. The statistical significance of differences in the penetration of photoacoustically delivered dye in gels was determined by a two-tailed Student's t-test. An unpaired t-test was used to analyze the data as each parameter varied. Differences were considered significant at $p \leq 0.05$.

3. Results

A. Spatial Distribution Measurement

For simplicity, most of experiments were conducted on the samples with planar geometry. A cylindrical geometry was used to simulate the boundaries of vessel walls and to show the clinical possibilities of photoacoustic drug delivery. The effects of laser parameters on photoacoustic drug delivery were qualitatively the same for planar and cylindrical geometries, but the penetration was less in the cylindrical case. We defined w and w^{coax} as stained width (Fig. 2). The parameters h_{mix}, h_{crack}, h_{mix}^{coax}, and h_{crack}^{coax} were defined as penetration.

1. *Planar Geometry*

The spatial distribution measurements are summarized in Table 1. As the parameters increased, some increased the penetration (laser energy, absorption coefficient, and pulse number), some decreased the penetration (gelatin strength, fiber size, and the one parameter had no significant effect on penetration (repetition rate).

Both penetration depths h_{mix} and h_{crack} increased significantly with increases in laser energy, absorption, and number of pulses. The penetration h_{mix} increased linearly, and h_{crack} increased with a steadily increasing slope. The stained width w was relatively independent of the laser energy and absorption coefficient, but it increased significantly as the number of pulses increased.

Increasing the gelatin strength, spot sizes, and the distance between a fiber tip and target surface caused both the penetration and the stained width to decrease significantly. Linear decreases in h_{mix} were observed, whereas h_{crack} decreased with steadily decreasing slope for each parameter. We found that the colored oil was easily driven into the low-strength gel samples following irradiation. For example, the colored oil was driven into the weaker gel (60 bloom) after one or two pulses, but at least five pulses were needed to push the colored oil into the stronger gel samples (300 bloom). We observed that during irradiation with a 300-μm fiber the solution was explosively ejected and the solution in front of the fiber tip became dark, i.e., it was burnt. Irradiation with a 600-μm fiber was more violent than that with a 1000-μm fiber, but no explosive ejection was observed. The repetition rate did not affect the penetration ($p = 0.15$–0.95) or the stained width ($p < 0.4$) significantly.

2. *Cylindrical Geometry*

A cleaved fiber tip (300 μm in core diameter) was used to deliver 50 laser pulses of 30 mJ at 3 Hz into the light-absorbing liquid (300 cm^{-1}) coaxially. The target was 3.5% gelatin (175 bloom). After laser irradiation the lumen area increased to 125%, and the colored oil was driven into the gels up to 1.5 mm [h_{crack}^{coax} in Fig. 2(b)]. The maximum depth h_{mix}^{coax} of a uniformly stained layer was less than 250 μm. The stained width w^{coax} of the wall was ~4 mm. One of these sectioned samples is illustrated in Fig. 3.

A side-firing fiber was also evaluated. The output spot size of this tip was ~700 μm in diameter. Fifty

Table 1. Spatial Distribution Measurements of Colored Oil in Gels with Planar Geometry[a]

Delivery Parameters							Measurements		
Energy (mJ)	Absorption Coefficient (cm^{-1})	Number of Pulses	Gelatin Strength (Bloom)	Fiber Size (μm)	Fiber Position (mm)	Repetition Rate (Hz)	h_{mix} ±0.05 (mm)	h_{crack} ±0.2 (mm)	w ±0.2 (mm)
30 → 100	300	10	175	1000	1	3	0.12 → 0.18	0.1 → 0.5	2.0 → 2.3
60	50 → 300	10	175	1000	1	3	0.07 → 0.15	0.0 → 0.4	1.9 → 2.0
60	300	10 → 100	175	1000	1	3	0.15 → 0.53	0.4 → 1.9	2.0 → 2.8
60	300	10	60 → 300	1000	1	3	0.25 → 0.10	0.8 → 0.2	2.1 → 1.5
60	300	10	175	300 → 1000	1	3	0.18 → 0.15	1.0 → 0.4	3.2 → 2.0
60	300	10	175	1000	1 → 5	3	0.15 → 0.06	0.4 → 0.0	2.0 → 1.0
60	300	10	175	1000	1	1 → 10	0.13 → 0.16	0.1 → 0.4	1.8 → 2.1

[a]All data are mean ± standard deviation of five samples.

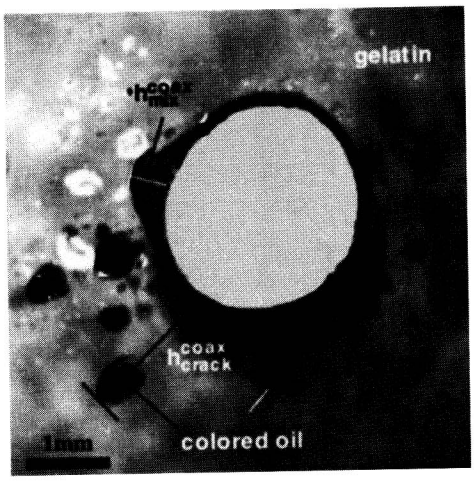

Fig. 3. Top view of colored-oil distribution in a 2-mm channel through gelatin (175 bloom) with cylindrical geometry after 50 pulses of 30-mJ laser energy through a 300-μm core-diameter fiber in 300-cm^{-1} colored oil. The laser energy was delivered coaxially. Extensive shadows are present because this section was 2 mm thick.

laser pulses of 40 mJ at 3 Hz were delivered. The corresponding radiant exposure is 104 mJ/mm^2. The penetration was comparable with that of planar geometry for the same laser parameters. The measurements revealed that the deeper penetration was more easily achieved by side delivery than by coaxial delivery. The light photomicrography in Fig. 4 illustrates that the colored oil is deeply driven into the gel (~1 mm) on the light-delivery side and only superficially (<100 μm) elsewhere.

B. Visualization of Photoacoustic Drug Delivery

In Fig. 5 a series of pictures shows the process of photoacoustic drug delivery on a gelatin sample (175 bloom) with planar geometry. The bubbles were formed in colored oil (300 cm^{-1}) with 30-mJ pulses delivered through a 300-μm core-diameter fiber. This corresponds to a laser radiant exposure of 424 mJ mm^2. The fiber tip was positioned 1 mm above the target. The camera flash occurred 25–1500 μs after the laser pulse. The cavitation bubble initially grew and interacted with the nearby gel. The maximum horizontal diameter of the bubble measured 2.4 mm and was reached at 110 μs. At ~250 μs after the laser pulse the bubble shrank to a minimum size and then rebounded slightly. A second maximum was observed at ~300 μs, and the bubble then shrank until ~415 μs. At ~500 μs a larger and less distinct shadow was seen, which may correspond to a final rebound of the bubble. This bubble size oscillation was reproducible. The bubble started its final collapse to the gel at ~650 μs, and the maximum penetration into the gel was reached at ~1 ms. The shape of the bubbles was not reproducible after the second rebound of the cavitation bubble. Evidently, the colored oil was driven into the gel as the result of the expansion and collapse of the bubble, and the deeper penetration of colored oil in gels was achieved following the collapse. We observed that the colored oil was pushed back to the surface because of the resistance of gels when the gels with higher mechanical strength (e.g., ≥175 bloom) were used during single-pulse irradiation. This is seen at 1.5 ms.

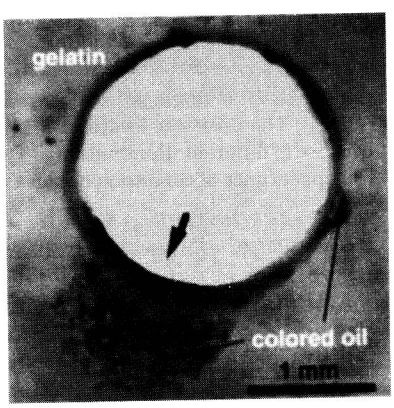

Fig. 4. Top view of colored-oil distribution in a 2-mm channel through gelatin (175 bloom) with cylindrical geometry after 50 pulses of 40-mJ laser energy through a side-firing fiber in 300-cm^{-1} colored oil. The laser energy was delivered perpendicular to the channel wall, as indicated by the arrow.

Photoacoustic drug delivery on a gelatin sample (175 bloom) with cylindrical geometry is shown in Fig. 6. In this experiment a 30-mJ laser pulse was delivered through a 300-μm core-diameter fiber into colored oil with absorption coefficient 300 cm^{-1}. The channel wall was dilated during the cavitation bubble expansion. The maximum dilation was reached after ~100 μs and amounted to 120% of the initial channel diameter. During the bubble collapse the channel wall invaginated, and the solution in the channel was pushed away from the fiber tip in both lateral and forward directions, which caused dilation and invagination along the channel wall until the end of the event. It took approximately 5 ms for the channel to return its original shape after a laser pulse. The minimum diameter was ~90% of the original value. We took the images on one sample rather than on a fresh sample each time to avoid misinterpretation of initial intrasample defects before irradiation.

Figure 7 shows a cavitation bubble developing between the side-firing fiber tip and the surface of the cylindrical channel after the delivery of a 40-mJ-energy laser pulse. The corresponding radiant exposure is ~104 mJ/mm^2. The other parameters were the same as those in Fig. 6. The images were recorded between 25 μs and 1 ms after laser radiation. The cavitation bubble was formed directly on the side surface of the fiber tip where the laser energy was absorbed. The maximal development of the laser-induced elliptical cavitation bubble is seen at 100 μs after the laser pulse. The corresponding bubble diameter and height were 1.7 and 1.2 mm, respectively. The bubble reached its minimum size at 250 μs and penetrated ~1.5 mm into the gelatin at ~1 ms. No bubble oscillation was observed. The

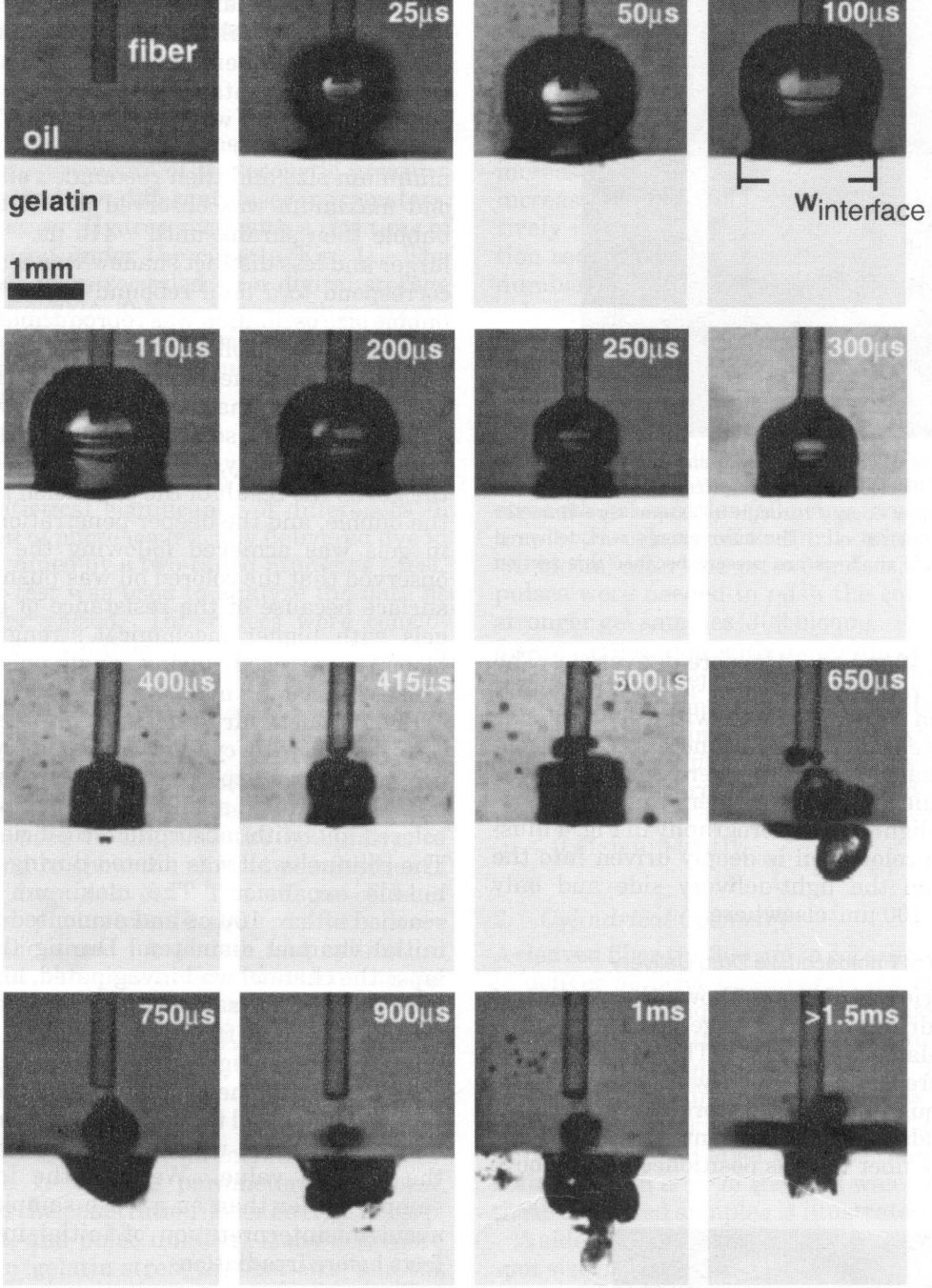

Fig. 5. Side views of photoacoustic drug delivery on gelatin (175 bloom) with a planar geometry. A single pulse of 30-mJ laser energy was delivered through a 300-μm diameter fiber. The absorption coefficient was 300 cm^{-1}. The fiber was located 1 mm above the gel surface. The backgrounds of four photographs (300–500 μs) are lighter than the rest because of different illumination. The bubble size was reproducible to 5% before the second rebound of the cavitation bubble (500 μs). The appearance of cavitation bubbles varied widely after 500 μs.

bubble did not penetrate the channel wall when the laser pulse was less than a 5 mJ. The bubble penetrated deeper into the gel at higher laser energies (i.e., >40 mJ). No displacement of the tip was observed during the irradiation. In this experiment the distance between the bubble site and the target was ~400 μm, and the gelatin was as thick as 4 mm. The initial channel wall surface was as not so smooth as a planar surface and was often associated with some defects. These differences may contribute to the differences in the bubble formation in Figs. 5 and 7, although the spatial distribution measurements were comparable. The images were taken on one sample, as explained above.

Flash photography also led to the following observations (pictures not shown): (1) Increasing energy,

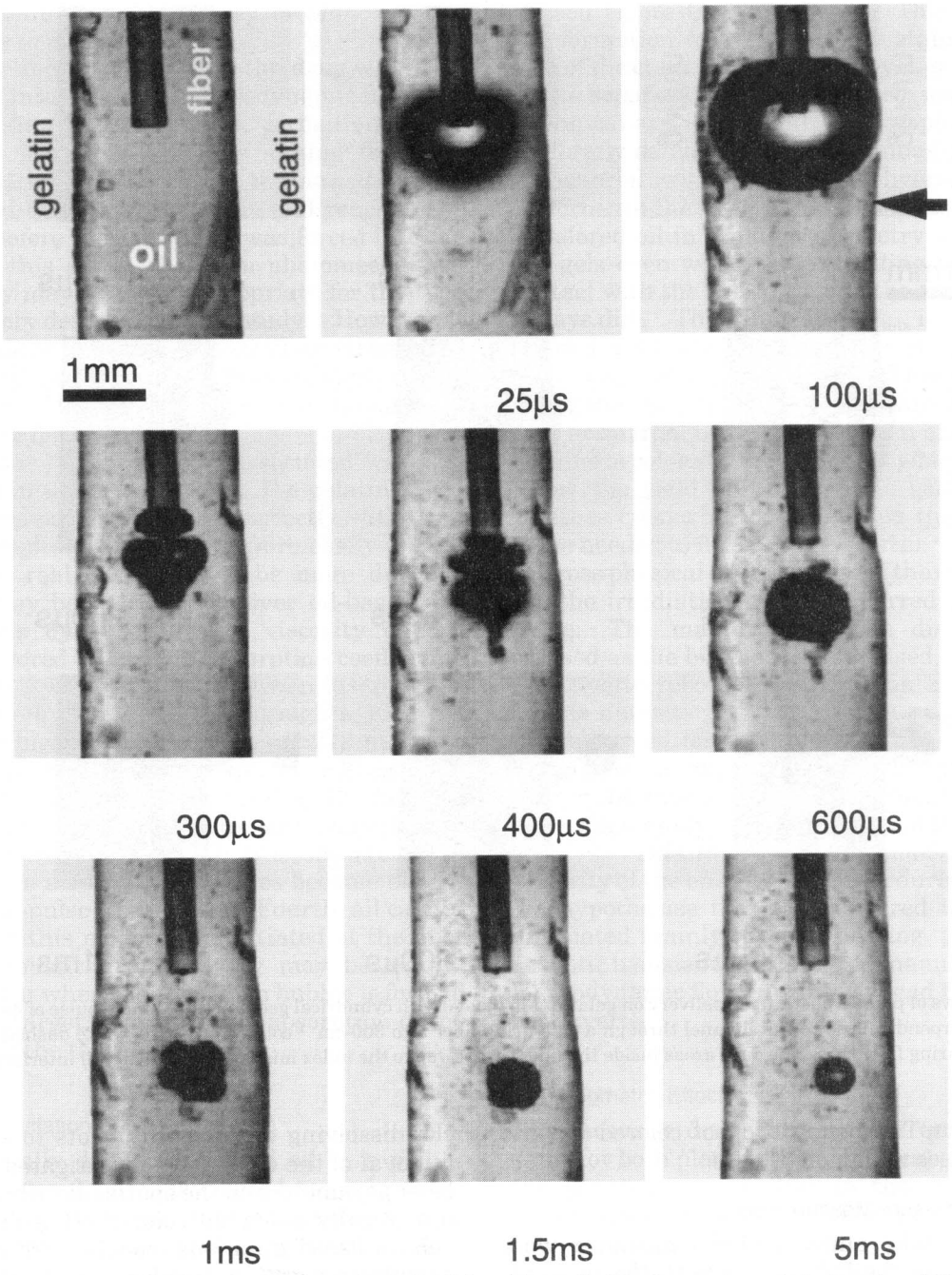

Fig. 6. Side views of photoacoustic drug delivery on gelatin (175 bloom) in a cylindrical geometry. A single pulse of 30-mJ laser energy was delivered through a 300-μm diameter fiber into 300-cm^{-1} colored oil. The absorption coefficient was 300 cm^{-1}. The laser energy was delivered coaxially. The arrow indicates the place where the deepest penetration was observed.

absorption coefficient, and radiant exposure increase the bubble size and the penetration of colored oil in the gel and delay the time of the maximum bubble size. For example, the bubble diameter was 2.7 mm at 110 μs when a 100-mJ laser pulse was delivered into the solution (300 cm^{-1}) through a 1000-μm fiber positioned 1 mm above the target, whereas it was 1.6 mm at 45 μs as 30 mJ of energy was delivered instead. (2) Increasing the target strength does not affect the bubble size unless the expanding bubble interacts with the target. If this occurs both the bubble size and the penetration of colored oil are reduced. (3) Increasing the distance between the fiber tip and the target decreases the penetration of colored oil in the gel, creates larger cavitation bubbles, and delays the time of the maximum bubble size. (4) Cavitation bubbles formed in cylindrical channels were smaller than those formed in unbounded solutions because of the boundary effect. (5) Multiple pulses affect the bubble formation—sometimes making the bubbles smaller, sometimes larger compared with the bubbles generated by

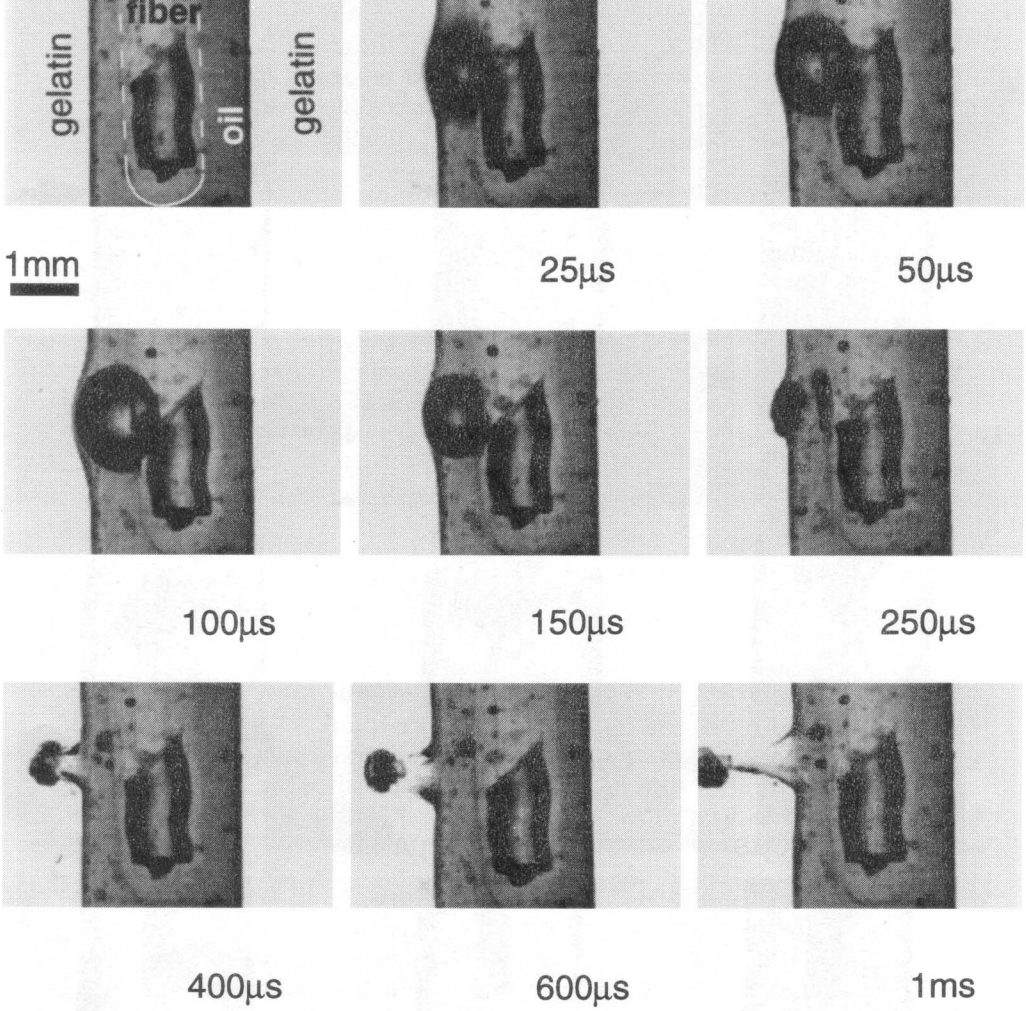

Fig. 7. Side views of photoacoustic drug delivery on gelatin (175 bloom) with cylindrical geometry. A single pulse of 40-mJ laser energy was delivered perpendicularly to the channel through a side-firing fiber into 300-cm^{-1} colored oil. The white dashed curve shows the edge of the side-firing fiber tip. The dark areas inside the fiber tip are due to the index mismatch at the air–oil interface.

single pulses. The penetration of colored oil into the gel increases with more pulses.

C. Acoustic Pressure Measurement

Flash photography and a PVDF transducer were used to correlate the bubble size with the pressure transients. The acoustic measurements were qualitative, and the measured pressure might be underestimated because of the slow response of the transducer and the multiple boundaries between the initial acoustic event and the transducer. We observed that the acoustic pressure transients were proportional to the bubble size and that bubbles of similar size created by different-size fibers generated similar maximum acoustic pressure transients. The acoustic measurements provided a quick qualitative check of the maximum bubble size observed visually.

4. Discussion

The major objective of this study was to investigate the feasibility of a photoacoustic technique to deliver clot-dissolving enzymes into clots to enhance laser removal of the clots. We investigated the effects of laser parameters on the spatial distribution of photoacoustically delivered colored oil (a drug model) in gelatin-based thrombus models. We used clear gel samples covered with colored oil to determine the spatial distribution of delivered drug. A stained area in the clear gel indicated the presence of colored oil delivered photoacoustically. No dye passively diffused into the clear water-based gels. The colored oil was driven into the gels following irradiation, cavitation bubble formation, and secondary acoustic emission. When no cavitation bubble was formed, no gelatin was stained. Normally, deeper penetration was accompanied by louder popping sounds. Acoustic pressure transients were detected during the expansion and collapse of the cavitation bubble. The spatial measurements also revealed that higher pressures resulted in deeper penetration. These findings suggest that cavitation bubble formation is crucial in photoacoustic drug delivery and that acoustic events can be used as a

means of monitoring the efficacy of photoacoustic drug delivery *in vivo*.

This study demonstrated that the drug was most likely driven into the clot by hydrodynamic flow that was due to the cavitation bubble formation rather than by the acoustic transients arising from the bubble formation, inasmuch as the acoustic transients passed through the sample and reached the transducer before the colored oil was forced into the gelatin. In this sense, the term photomechanical drug delivery may be more appropriate for the type of drug delivery described in this study. However, it remains unclear whether the acoustic transients contribute to the delivery through other mechanisms that might weaken the gelatin before the onset of hydrodynamic flows.

At least four limitations are associated with the models used in this study. First, the gelatin-based thrombus models did not work perfectly with multiple-pulse studies because they were easily melted or fractured; real clots tend to be more durable. Second, it may be harder to deliver oil-based dye than aqueous dyes because of viscosity effects. Third, the colored oil at high absorption coefficients (e.g., 300 cm^{-1}) was easily burnt when laser pulses with high energy (e.g., 100 mJ through a 1000-μm core fiber) or high radiant exposure ($\geq$212 mJ/mm^2 or, say, 60 mJ through a 600-μm core fiber) were used. The burnt solution surrounding the fiber tip sometimes caused the photoacoustic delivery process to become nonreproducible. It was observed that the color of the solutions sometimes became darker after multiple-pulse irradiation. Fourth, all cavitation events in this model were initiated at the fiber tip. Photoacoustic drug delivery may be significantly different when the cavitation bubble is formed directly on a target because of the absorption of the laser pulse by the target.

A. Effect of Cavitation Bubble Formation

Photoacoustically delivered colored oil in a planar geometry was uniformly distributed as an inverted hemisphere layer and in a cylindrical geometry as a ball-shaped profile. The uniformly stained layer looked like a dye–gelatin mixture (i.e., the gel itself rather than small colored-oil droplets became stained) under light microscopy and could not be washed away by clear oil or wicked off by a piece of tissue paper. Colored cracks were formed below the uniformly stained layer.

The shape of colored cracks was not reproducible, and the cracks were not always associated with the uniformly stained layers. For example, no colored cracks (i.e., $h_{crack} = 0$) were formed by ten 60-mJ laser pulses through a 1000-μm core fiber in a colored oil (50 cm^{-1}), but colored cracks 400 μm in depth were formed by the same laser parameters when a different colored oil (300 cm^{-1}) was used (see Table 1). Light microscopy showed that the cracks were formed as the result of defects in gel structure. No defects were observed in the positions where the cracks were formed before the irradiation. This suggests that the formation of the uniformly stained layers and that of the cracks are mediated by separate processes. These separate processes can be used to advantage in clinical applications. For example, drugs can be uniformly delivered into a thrombus or deposited in an arterial wall or deeply delivered into plaque underneath the thrombus by fracture.

Colored oil in a planar geometry was driven into the gels even when the expanding bubbles had no contact with the gels (although the collapsing bubble always did). The penetration h_{mix} increased but the stained width w remained relatively constant when h_{crack} was zero [cf. Fig. 2(a)]. These observations imply that h_{mix} depends on the hydrodynamic forces that arise from both the expansion and the collapse. A uniform colored layer is formed when the forces are below the yield strength of the gelatin structure, whereas cracks are formed when the forces exceed those needed to fracture the gelatin.

Gross physical displacement of the cuvette containing the irradiation targets occurred after the laser pulse. The magnitude of the displacement increased as the bubble size increased. For example, the cuvette rebounded more than 2 mm when the bubble diameter was ~4 mm, but no displacement was observed for a 1.3-mm bubble. The direction was opposite that of laser delivery. The bubble energy obtained with Rayleigh's bubble formula[15,19,20] accounts for only a small fraction of the laser energy (<0.1%). This raises the question: How was the majority of the energy dissipated during the process? We hypothesize that the delivered laser energy is dissipated mainly through heating, phase changes, acoustic transients, and hydrodynamic flow of liquid. Hydrodynamic flows ultimately lead to movement of the cuvette.

B. Geometric Effect

Photoacoustic drug delivery was qualitatively the same for both planar and cylindrical geometries, but the penetration was less in the cylindrical case. Flash photography showed that the fiber tip affected the cavitation bubble growth: bubbles grew faster in the radial and forward directions. The bubble did not move radially and migrated away from the fiber tip on collapse. Strong hydrodynamic flows were associated with the bubble collapse and may be the reason that deeper penetration was achieved by perpendicular delivery rather than by coaxial delivery. Collapsing bubbles migrated toward the target in both perpendicular and side-firing delivery (see Figs. 5 and 7). This finding suggests that the side-firing light-delivery devices may be promising for photoacoustic drug delivery in vascular applications.

No mass removal was observed for the samples with planar geometry. However, in a cylindrical geometry light microscopy revealed that the lumen size increased by as much as 1.5 mm after multiple pulses. We hypothesize that gelatin removal in the cylindrical channel is due to hydrodynamic flow and

erted directly on the planar surface, and the flow passed over the channel surface in a cylindrical geometry. Melted gelatin may resolidify at the planar surface, whereas in a cylindrical geometry the melted gelatin may be carried away.

When the laser pulses were delivered perpendicularly, the deepest penetration was observed in front of the fiber tip. In a channel with coaxial delivery the deepest penetration was inside the channel wall ~1 mm from the distal face of the fiber (see Fig. 6). This most likely is the result of bubbles' propagating away from the fiber face. Also, bubble movement may be a reason that w^{coax} was ~4 mm long.

The presence of boundaries reduced the maximum size of the cavitation bubble. For example, a 30-mJ laser pulse delivered through a 300-μm fiber created a 1.9-mm-diameter bubble in a 2-mm-diameter channel filled with a 300-cm^{-1} colored oil (Fig. 6), but a 2.9-mm bubble was created in an unbounded colored oil at the same energy (picture not shown). To estimate the energy lost to the dilatation of the channel wall after a 30 mJ laser pulse, we compared the maximum bubble radius in both cases, using Rayleigh's bubble formula. The result indicated that ~30% of the bubble energy was dissipated in the dilatation process.

C. Multiple-pulse Effects

A surprising observation was that the stained width on the surface was relatively independent of the laser energy and absorption coefficient when laser pulses were delivered perpendicularly. The interface ($w_{interface}$ in Fig. 5) was smaller than the stained width w [Fig. 2(a)] for single-pulse events. Flash photography revealed that the cavitation bubble sizes varied during the multiple-pulse irradiation. This phenomenon was supported by the acoustic pressure measurements. Sometimes the amplitude of acoustic signals during multiple pulses was ten times that of a single pulse, and at other times no signal was detected. The variation in bubble size and acoustic transient amplitude is possibly not caused by the changes in the laser pulse energy when multiple pulses were delivered, because the variation was less than 5%. The independence of the stained width from laser energy and absorption coefficient seems to be a side effect of multiple pulses.

The effect of multiple pulses on both the penetration and the stained width was significant (see Table 1). We found that the deeper penetrations, especially h_{crack} and h_{crack}^{coax}, were more easily achieved by multiple pulses than by the combinations of other laser parameters. Sequential bubble collapses likely weakened the gelatin structure, and the colored oil was easily driven into fractured lines.

We observed that, when the gelatin strength was greater than 60 bloom, colored oil could not be deposited upon the gel surface with a single pulse. This finding suggests that the oil entrainment may be caused by mechanical rather than

despite a high initial temperature of the cavitation bubble (above 300 °C calculated by a partial vaporization theory[21,22]). Presumably significant cooling has occurred by the time the bubble reaches the gelatin surface. Mechanical vibration owing to the hydrodynamic forces has been shown to liquefy gelatin.[23] However, the thermal effect may contribute to melting during multiple-pulse irradiation because of successive amounts of heat deposited upon the gelatin surface with each bubble expansion.

Multiple-pulse variation of bubble dimensions has been reported by van Leeuwen *et al.*[24] A new observation made in our study is that small gas bubbles (<50 μm) around the fiber tip played an important role in the bubble dynamics. After a laser pulse, long-lasting (several seconds) small gas bubbles were often formed around the fiber tip. Cavitation bubble size was reproducible when no gas bubbles were present; otherwise the cavitation bubble size could change significantly. This finding suggests that the use of a degassed solution may reduce the effect of multiple pulses on the bubble dynamics, although, of course, this is impossible in an *in vivo* environment.

D. Similar Effects

The same radiant exposure produces different-sized bubbles when different-sized fibers are used. Furthermore, the same pulse energy with different-sized fibers also produces different-sized bubbles. However, similar maximum cavitation bubble sizes can be produced by different sets of laser parameters. For example, a cavitation bubble 3.2 mm in diameter can be produced in unbounded colored oil (300 cm^{-1}) by a 300-μm fiber at 33 mJ, by a 600-μm fiber at 50 mJ, or by a 1000-μm fiber at 100 mJ, with an error estimate of less than 5%. The maximum acoustic signals were similar for similar bubble sizes. Similar spatial distributions of colored oil in gels were achieved with the three sets of parameters mentioned above when the fibers were located 1 mm above the gelatin (175 bloom) samples.

Alternatively, 60-mJ laser energy delivered by a 1000-μm fiber and ten additional pulses (data not shown) also can be used instead of 100-mJ laser energy to yield equal penetration. These findings suggest that similar drug delivery can be achieved by various combinations of laser parameters. Furthermore, photoacoustic drug delivery may be safer in a smaller laser-delivery catheter because one can use a lower energy to achieve equivalent penetration by using more pulses.

Cavitation bubble formation in this study is similar to that of a Q-switched holmium laser in water. The absorption coefficient of water at 2.1 μm is 30 cm^{-1}. The Q-switched pulse length is ~1 μs and is therefore comparable with those used in this study. In this study and in those of Jansen *et al.* the cavitation bubbles are formed at the fiber tip after the laser pulse owing to the laser energy absorption by the liquid.[22] The Q-switched holmium laser can

be used for photoacoustic drug delivery, although Table 1 indicates that the penetration will be half that of a 577-nm pulsed dye laser in blood (absorption coefficient of 300 cm^{-1}). The pulse duration for the free-running holmium laser is much longer (~250 μs), and the bubble dynamics are completely different because the cavitation bubble is formed during the laser pulse.

In conclusion, we have demonstrated the feasibility of photoacoustic drug delivery to drive drugs (colored oil) into thrombus (a gelatin-based model). The results of this study indicate that cavitation bubble formation is the governing mechanism for photoacoustic drug delivery with microsecond laser pulses in light-absorbing liquids. When no cavitation bubble was formed, no gelatin was stained. There are two processes in photoacoustic drug delivery: the formation of uniformly stained layers and the formation of colored cracks. The two separate processes may benefit clinical applications. The deepest penetration of colored oil in gels follows the cavitation bubble collapse. The penetration was less than 500 μm when the gelatin structure was not fractured, and the colored oil could be driven a few millimeters into the gels in both axial and radial directions. The results of this study demonstrated that similar penetration could be achieved by use of various combinations of laser parameters.

Address any correspondence to S. A. Prahl at Oregon Medical Laser Center.

We thank U. S. Sathyam and M. J. Girsky for their valuable comments on the manuscript. This research was supported in part by the Murdock Foundation, Portland, Ore., and the Whitaker Foundation, Washington, D.C.

References

1. D. A. Dichek, R. F. Neville, J. A. Zwiebel, S. M. Freeman, M. B. Leon, and W. F. Anderson, "Seeding of intravascular stents with genetically engineered endothelial cells," Circulation **80,** 1347–1353 (1989).
2. E. G. Nabel, G. Plautz, and G. J. Nable, "Site-specific gene expression in vivo by direct gene transfer into the arterial wall," Science **249,** 1285–1288 (1990).
3. H. Lin, M. S. Parmacek, G. Morle, S. Bolling, and J. M. Leiden, "Expression of recombination genes in myocardium in vivo after direct injection of DNA," Circulation **82,** 2217–2221 (1990).
4. E. C. Santoian, M. B. Gravanis, K. Anderberg, N. A. Scott, S. P. Karas, J. E. Schneider, and S. B. King III, "Use of a porous infusion balloon in swine coronary arteries: low pressure minimizes arterial damage," Circulation **84,** II-591 (1991).
5. A. Fernńdez-Ortiz, B. J. Meyer, A. Mailhac, E. Falk, L. Badimon, J. T. Fallon, V. Fuster, J. H. Chesebro, and J. J. Badimon, "A new approach for local intravascular drug delivery: iontophoretic balloon," Circulation **89,** 1518–1522 (1994).
6. H. Wolinsky and M. B. Taubman, "Local delivery to the arterial wall: pharmacologic and molecular approaches," in *Coronary Balloon Angioplasty,* R. E. Vlietstra, ed., (Blackwell Scientific, Lakeland, Fla., 1994), pp. 156–186.
7. A. M. Lincoff, E. J. Topol, A. Frieser, and S. G. Ellis, "Local drug delivery for prevention of restenosis," Circulation **90,** 2070–2084 (1994).
8. H. Shangguan, L. W. Casperson, A. Shearin, K. W. Gregory, and S. A. Prahl, "Photoacoustic drug delivery: the effect of laser parameters on spatial distribution of delivered drug," in *Laser-Tissue Interaction VI,* S. L. Jacques, ed., Proc. SPIE **2391,** 394–402 (1995).
9. H. Shangguan, L. W. Casperson, A. Shearin, and S. A. Prahl, "Visualization of photoacoustic drug delivery dynamics," Lasers Surg. Med. **S7,** 4–5 (1995).
10. R. C. Zeimer, B. Khoobehi, and R. L. Magin, "A potential method for local drug and dye delivery in the ocular vasculature," Invest. Ophthalmol. Vis. Sci. **29,** 1179–1183 (1988).
11. T. J. Flotte, S. Lee, H. Zhang, D. MacAuliffe, T. Douki, and A. Doukas, "Laser-induced stress transients: Applications for molecular delivery," in *Laser-Tissue Interaction VI,* S. L. Jacques, ed., Proc. SPIE **2391,** 202–207 (1995).
12. K. W. Gregory and R. R. Anderson, "Liquid core light guide for laser angioplasty," IEEE J. Quantum Electron. **26,** 2289–2296 (1990).
13. T. G. van Leeuwen, M. J. van der Veen, R. M. Verdaasdonk, and C. Borst, "Noncontact tissue ablation by holmium: YSGG laser pulses in blood," Lasers Surg. Med. **11,** 26–34 (1991).
14. A. Vogel, R. Engelhardt, and U. Behnle, "Minimization of cavitation effects in pulsed laser ablation—illustrated on laser angioplasty," Appl. Phys. B **62,** 173–182 (1996).
15. K. Rink, G. Delacrétaz, and R. P. Salathé, "Fragmentation process of current laser lithotriptors," Lasers Surg. Med. **16,** 134–146 (1995).
16. A. A. Oraevsky, R. Esenaliev, S. L. Jacques, and F. K. Tittel, "Laser flash photography of cold cavitation-driven ablation in tissues," in *Laser-Tissue Interaction VI,* S. L. Jacques, ed., Proc. SPIE **2391,** 300–307 (1995).
17. K. Gregory, "Laser thrombolysis," in *Interventional Cardiology,* E. J. Topol, ed. (Saunders Company, Philadelphia, Pa., 1994), Vol. 2, Chap. 5, pp. 892–902.
18. C. W. Francis, A. Blinc, S. Lee, and C. Cox, "Ultrasound accelerates transport of recombinant tissue plasminogen activator into clots," Ultrasound Med. Biol. **21,** 419–424 (1995).
19. O. M. Rayleigh, "On the pressure developed in a liquid during the collapse of a spherical cavity," Philos. Mag. **34,** 94–98 (1917).
20. A. Vogel, S. Busch, K. Jungnickel, and R. Birngruber, "Mechanisms of intraocular photodisruption with picosecond and nanosecond laser pulses," Lasers Surg. Med. **15,** 32–43 (1994).
21. T. G. van Leeuwen, E. D. Jansen, M. Motamedi, C. Brost, and A. J. Welch, "Excimer laser ablation of soft tissue: a study of the content of rapidly expanding and collapsing bubbles," IEEE J. Quantum Electron. **30,** 1339–1345 (1994).
22. E. D. Jansen, T. G. van Leeuwen, M. Motamedi, C. Brost, and A. J. Welch, "Partial vaporization model for pulsed mid-infrared laser ablation of water," J. Appl. Phys. **78,** 564–571 (1995).
23. G. K. Batchelor, *Introduction to Fluid Dynamics* (Cambridge U. Press, Cambridge, 1980).
24. T. G. van Leeuwen, L. van Erven, J. H. Meertens, M. J. Post, and C. Borst, "Vapor bubble expansion and implosion: the origin of 'mille feuilles'," in *Diagnostic and Therapeutic Cardiovascular Interventions III,* G. S. Abela, ed., Proc. SPIE **1878,** 2–12 (1993).